JOURNAL OF CATALYSIS **169,** 490–502 (1997)
ARTICLE NO. CA971705

Nanophase Fluorite-Structured CeO_2–ZrO_2 Catalysts Prepared by High-Energy Mechanical Milling

Analysis of Low-Temperature Redox Activity and Oxygen Storage Capacity

Alessandro Trovarelli,* Francesca Zamar,* Jordi Llorca,† Carla de Leitenburg,* Giuliano Dolcetti,* and Janos T. Kiss‡

*Dipartimento di Scienze e Tecnologie Chimiche, Università di Udine, via Cotonificio 108, 33100 Udine, Italy; †Departament de Quimica Inorgànica, Universitat de Barcelona, Diagonal 647, 08028 Barcelona, Spain; and ‡Department of Organic Chemistry, Jozsef Attila University, Szeged, Dom ter 8, H-6720, Hungary

Received January 2, 1997; revised March 12, 1997; accepted March 12, 1997

The utilization of mechanical milling for the preparation of catalysts based on ceria structurally modified with zirconia is presented. It is shown that room-temperature high-energy ball milling is an effective tool for the synthesis of nanophase CeO_2–ZrO_2 solid solution in a wide composition range. The use of combined X-ray diffraction analysis, Raman spectroscopy, and electron microscopy indicate that the milling process induces the formation of true solid solutions with a contraction of the cell parameter for cubic ceria following the introduction of Zr into the lattice. This, in turn, remarkably enhances the oxygen storage/transport and redox capacity compared to pure ceria and zirconia or to a simple mixture thereof. An unusual resistance to high-temperature cycling was also evidenced. These features were analyzed by the study of the reduction profile of doped ceria carried out by temperature-programmed reduction at different milling times. The oxygen storage capacity (OSC) of the catalysts was also evaluated; both the total and the kinetic accessible OSC indicated that the best composition is $Ce_xZr_{1-x}O_2$ with $x > 0.5$. This was correlated to the structural features and to the presence of a high concentration of ions with redox character (i.e., Ce^{4+} ions) which favor oxygen mobility.

INTRODUCTION

Materials containing ceria have been the subject of thorough investigation in recent years because of their usefulness in a number of applications in different areas of chemistry. One such area is catalysis, where ceria is currently being used as an active component in the so-called *three-way catalysts* for automotive exhaust treatment as well as in several other catalyst formulations (1, 2). One of the most important roles of CeO_2 in these multicomponent systems is to provide surface active sites and to act as an oxygen storage/transport medium by shifting between Ce^{3+} and Ce^{4+} under reductive and oxidizing conditions, respectively. These redox properties are strongly enhanced if foreign cations such as Zr (3, 4), Gd (5), Pr (6), Tb (7), and Pb (8) are introduced into the CeO_2 lattice by forming solid solutions. This is the result of enhanced oxygen ion mobility inside the modified fluorite lattice originating from the formation of a defective, fluorite-structured solid solution in which cations of different radius and/or charge have replaced cerium atoms. Much effort has been focused on the preparation of these mixed oxides, which are potentially useful as catalysts for sensors, for carrying out selective oxidations, and for providing low ignition temperatures for catalyzed combustion reactions. The goal here is to lower the temperature required for O_2 diffusion through the catalyst, which could lead to greater catalyst efficiency at lower temperatures. However, further development of these materials requires detailed information on their structural features and above all a precise knowledge of the role of their various components and the influence of preparation procedure on redox behavior.

Special attention has been focused in recent years on the preparation of ceria structurally doped with ZrO_2. These materials show enhanced thermal (9), redox (3, 4, 7, 10), and catalytic properties (11, 12) compared to pure undoped ceria and their commercial development is being actively pursued, especially for the auto-exhaust market (13–15). Several approaches have been used to prepare these materials, from high-temperature calcination of a mixture of the oxides (3), which gives materials with very low surface areas, to coprecipitation followed by supercritical drying of the hydrogels to produce high surface area aerogels (16). High-energy mechanical milling (MM) has also been shown to be a promising technique for the generation of nanostructured metal and metal-oxide phases (17). MM consists of a high energy ball milling process that can be used to produce complex materials from a blend of elemental

0021-9517/97 $25.00

powders. Since its introduction in the early 1970s by Benjamin (18), there have been a number of *mechanochemical* studies of the synthesis of nonequilibrium structures and microstructures, including amorphous alloys, solid solutions alloys, nanocrystalline materials, intermetallic compounds, and metastable phases. Several treatments employing mills have been applied at various stages of mixed oxides preparation to enhance catalytic activity or selectivity (19–21), for example by changing sample morphology or by inducing surface modifications. Mixed oxides have also been prepared entirely by high-energy mechanical milling (22, 23) and recently mixed oxides containing CeO_2 and dopants such as ZrO_2, TbO_x, and HfO_2 have been specifically prepared for catalytic applications (7, 24).

The aim of this paper is to characterize the properties of CeO_2–ZrO_2 mixed oxides prepared by room-temperature high-energy mechanical milling of cubic CeO_2 and monoclinic ZrO_2. Particular attention was paid to the kinetic of the milling process and to the structural/morphological features of the final material. Redox behavior of the catalysts was investigated in depth, with special focus on oxygen storage capacity, both the total and the kinetically limited. These studies yielded unambiguous evidence for the formation of a mixed-oxide phase in a wide composition range by milling the pure oxides at room temperature. Finally, and in agreement with recent findings, the redox and oxygen storage properties of ceria are strongly enhanced if Zr is introduced into the CeO_2 lattice, especially when the dopant level does not exceed 50 mol%.

EXPERIMENTAL

Catalyst Preparation

CeO_2 (99.999%, surface area 5–18 m^2/g) was purchased from Aldrich and used as received. ZrO_2 was prepared by calcination of hydrous zirconia (MEL Chemicals) at 973 K (surface area 27 m^2/g). Preparation of the mixed oxides was carried out with a high-energy vibratory ball-mill (Spex 8000) at an oscillation frequency of 20 Hz and an amplitude of approximately 20 cm. Powders were loaded into a 50-ml ZrO_2 vial equipped with six Y-doped, high wear-resistant Zirconia balls (Ø 10 mm, Tosoh Corporation). The ball-to-powder ratio was 18/1 (i.e., 18 g of balls to 1 g of powder) and milling time ranged from 0.5 to 12 h.

Structural and Morphological Studies

Powder X-ray data were collected with a Siemens powder diffractometer using Cu$K\alpha$ radiation ($\lambda = 1.5418$ Å) by placing samples in aluminum sample holders. High-resolution powder XRD data for structural analysis were collected over a 14-h period from $2\Theta = 20$–75 with a 0.02° step size. Signals were fitted with Voigt functions and data were collected from the six main reflections of a fluorite-structured material corresponding to {111}, {200}, {220}, {311}, {222}, and {400} diffraction planes.

Samples for scanning electron microscopy analysis (SEM) were mounted on stubs and metalized with gold by a sputtering system device (S150A Edwards). They were observed by a Stereoscan 250 scanning electron microscope (Cambridge Instrument).

Conventional transmission electron microscopy combined with dispersive X-ray microanalysis (EDX) was carried out with a Hitachi H 800-MT electron microscope working at 200 kV and equipped with a Kevex analytical system. High-resolution electron microscopy (HREM) combined with EDX was performed using a Philips CM-30 electron microscope working at 300 kV (La_B6) with 0.20-nm point-to-point resolution and equipped with a Link analytical system. Samples were supported on carbon-coated gold or copper grids by depositing a drop of the specimen suspended in methanol. The sample was then transported to the microscope stage and the equipment was pumped down for several hours before observation. Magnification of HREM images and electron diffraction patterns were calibrated with pure CeO_2 ($a = 0.541$ nm) under the same electron optical conditions.

The Raman spectra were taken on a Bio-Rad Digilab Division dedicated FT-Raman spectrometer between 3500 and 70 cm^{-1} at 4 cm^{-1} optical resolution employing 500-mW energy of a Nd:YVO_4 excitation laser at the sample position. Glass capillary sample holders were used. The number of accumulated scans was 512. The spectra were processed employing the GRAMS/386-based software supplied with the FT-Raman spectrometer.

Textural properties were measured with a Carlo Erba Sorptomatic 1900 instrument using the BET method.

Oxygen Storage Capacity (OSC) and Redox Activity

Capacity to store and release oxygen was measured under conditions where both total and kinetic-accessible OSC can be detected. Total OSC was measured after reducing the catalyst (50 mg) at the appropriate temperature (650 K) under H_2 flow (2 h, 35 ml/min STP). Before measuring O_2 uptake, the catalyst after reduction was treated at 650 K under inert flow for 30 min, and then pulses of a mixture containing oxygen (1% O_2 in He) were injected up to the breakthrough point. Dynamic OSC was measured using pulses of oxygen (250 μl, 1% O_2 in He) and hydrogen (250 μl) alternately injected (every 3 min) into the catalyst bed at 650 K. OSC was evaluated from oxygen consumption in the first O_2 pulse following an hydrogen pulse.

Redox activity was measured by temperature-programmed reduction (TPR) experiments which were carried out by treating samples (50–70 mg) in a U-shaped quartz microreactor inserted into a furnace (300–1473 K, 10 K/min) with a mixture of 5% H_2 in Ar (35 ml/min STP) and by

monitoring H_2 consumption with a thermal conductivity detector. Quantitative calculations of the extent of reduction were performed by calibrating the apparatus for hydrogen consumption with reduction of CuO to Cu, as previously specified (25).

RESULTS AND DISCUSSION

Phase Composition of Mixed Oxides

Figure 1 reports the X-ray diffraction patterns of powders obtained by ball milling monoclinic ZrO_2 (50% mol) and cubic CeO_2 (50% mol). Diffractograms were collected after 0, 0.5, 2, 4, and milling for 9 h. The simple mixture of CeO_2 and ZrO_2 (i.e., without milling) showed an XRD pattern which is the sum of the diffractions of cubic CeO_2 and monoclinic ZrO_2. After milling for 2 h, a modification in the X-ray pattern indicated that a solid-state reaction had occurred. The main peaks relative to cubic CeO_2 and monoclinic ZrO_2 had partially disappeared and were replaced by broad signals, which are indicative of a modification of the crystal structure. After 9 h milling, the XRD pattern indicated the formation of a single-phase $Ce_{0.5}Zr_{0.5}O_2$ solid solution. Prolonged milling produced no further variations in the diffraction signals observed. This is clear from Fig. 2, where the diffraction peaks corresponding to the {220} plane are reported at a number of milling times. Profile (a), with a peak at 47.50°, corresponds to the difraction of the {220} plane of CeO_2 in a simple mechanical mixture

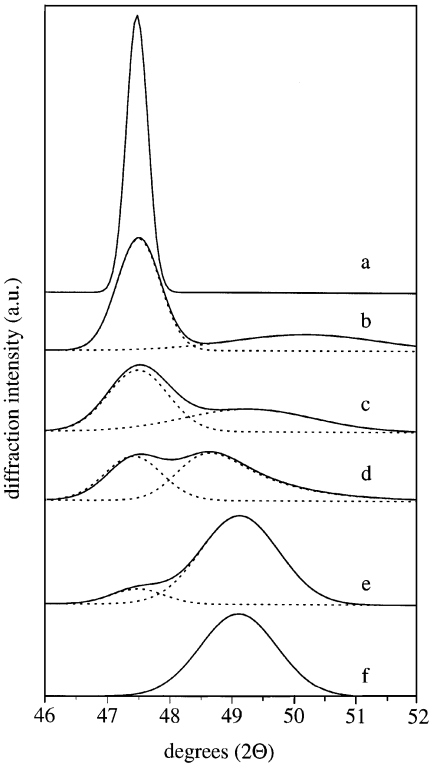

FIG. 2. Diffraction of {220} plane of cubic fluorite-structured material containing mixture of 50% mol CeO_2 and 50% mol ZrO_2 (a), the same milled for 0.5 h (b), 2 h (c), 4 h (d), 7 h (e), and 9 h (f). The peaks were fitted with Voigt functions (——) and deconvolution (- - -) was performed with PeakFit software.

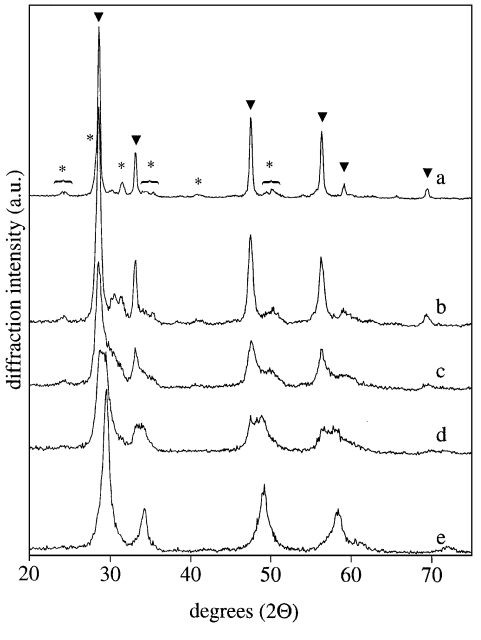

FIG. 1. X-ray diffraction patterns of mixture of 50% mol cubic CeO_2 (▼) and 50% mol monoclinic ZrO_2 (∗) milled for 0 h (a), 0.5 h (b), 2 h (c), 4 h (d), and 9 h (e).

of CeO_2 and ZrO_2. After 0.5 and 2 h milling, the intensity of this signal decreased and the growth of a new broad feature centered at higher values of 2Θ was observed. These modifications indicate that solid-state reaction induces a partial amorphization and/or a partial modification of crystal size and lattice parameters as a result of the mechanical impact of the powders with the balls. It has been reported that mechanical milling of powders induces fracture and deformations through high-energy collisions between balls and particles (17). This in turn leads to a modification of crystallite size also detected by transmission electron microscopy analysis (see below). After 9 h milling, the shape and position of the signal stabilized at a value of 49.20°. A complete X-ray analysis of the six main reflections indicated the formation of a cubic fluorite-structured cell with $a = 0.5243(5)$ nm.

Solid solutions with a CeO_2 molar content of 20% and 80% were obtained using the same methodology. The kinetic of the process, as revealed by X-ray diffraction, indicates that the transformation of starting materials into Ce–Zr–O solid solution is complete in about 9–11 h. Major peaks are indexed as a cubic fluorite-structured material with $a = 0.5336(8)$ nm for $Ce_{0.8}Zr_{0.2}O_2$ and $a = 0.5183(3)$ nm

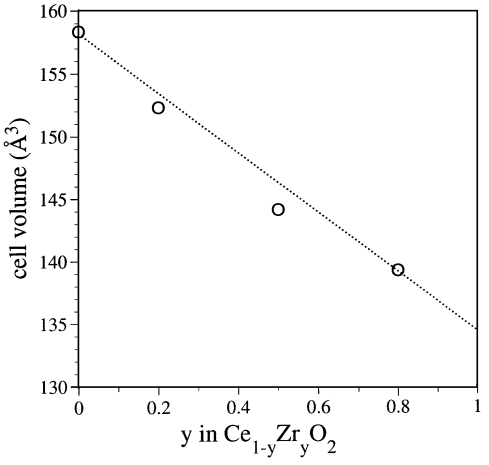

FIG. 3. Cell volume of (Ce,Zr)–O solid solutions obtained by milling ceria and zirconia for 9 h. Experimental values (○) vs values calculated using the empirical relationship developed in Ref. (26) (···).

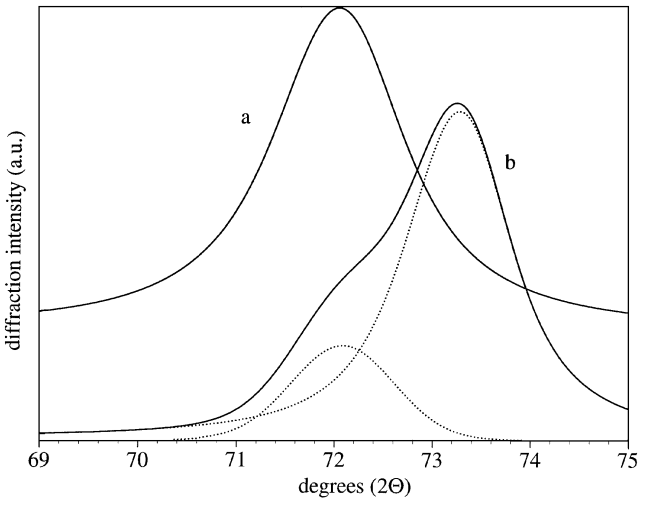

FIG. 4. Peak corresponding to diffraction of plane {400} in $Ce_{0.5}Zr_{0.5}O_2$ (a), and $Ce_{0.2}Zr_{0.8}O_2$ (b) obtained by ball-milling ceria and zirconia for 9 h. Solid lines represent the experimental signal fitted with Voigt functions ($r^2 = 0.994$), while dotted lines show the deconvolution profile of $Ce_{0.2}Zr_{0.8}O_2$.

for $Ce_{0.2}Zr_{0.8}O_2$. The XRD lines of the fluorite phases are extremely broad and in consequence the lattice constant cannot be accurately determined. However, the values obtained are in good agreement with those calculated by the empirical relationship developed by Kim for CeO_2–ZrO_2 (26), as may be seen in Fig. 3.

For the binary system Ce–Zr–O, there are three possible structures: monoclinic, tetragonal, and cubic; and several stable or metastable phases having tetragonal symmetry were found and separately characterized (27). At high CeO_2 concentrations ($CeO_2 > 80\%$ mol), the cubic phase is favored, whereas for ZrO_2-rich solid solutions the monoclinic phases are observed, although it is well established that cubic ZrO_2 is stabilized by incorporating a small amount of an oxide like Y_2O_3 or CaO. For intermediate composition both cubic and tetragonal phases were detected, and it is very difficult on the basis of X-ray diffraction experiments to distinguish between the two, owing to the small difference in the cell parameters. The structural analysis of $Ce_{0.2}Zr_{0.8}O_2$ deserves some additional comment with regard to the possible coexistence of the tetragonal and cubic phases in this sample. Peak analysis does not reveal any splitting of the {200}, {220}, and {311} signals but comparison of the diffraction of the {400} plane for $Ce_{0.2}Zr_{0.8}O_2$ and $Ce_{0.5}Zr_{0.5}O_2$ indicates the presence of an additional component at lower Θ values for $Ce_{0.2}Zr_{0.8}O_2$. Deconvolution of the XRD profile (Fig. 4) is consistent with the splitting of the peaks corresponding to the {004} and {400} planes at 72.08° and 73.24°, indicating a partial tetragonalization of the structure. Calculation of the cell parameters using these peaks shows that $a = 0.5165$ nm and $c = 0.5237$ nm with $c/a = 1.014$. Raman spectra collected in the region 100–900 cm^{-1} (Fig. 5) confirm these findings. The spectrum of pure ZrO_2 features several bands in this region which are attributable to monoclinic ZrO_2 (28), while one sharp single band (located at 465 cm^{-1}) and a very weak intensity scattering between 70 and 700 cm^{-1} characterize the Raman spectrum of pure CeO_2. Weak bands around 260 and 607 cm^{-1} and a shoulder near 405 cm^{-1} are also observed. The main peak at 465 cm^{-1} is due to the F_{2g} Raman active mode typical of a fluorite-structured material. The spectrum of $Ce_{0.8}Zr_{0.2}O_2$ features a sharp band at 465 cm^{-1} plus a strong intensity scattering in the region

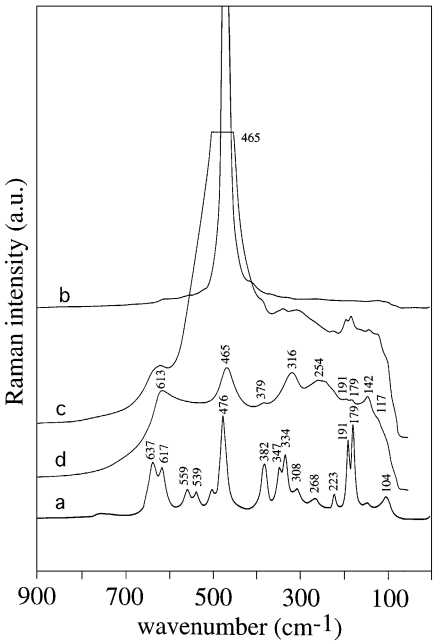

FIG. 5. Raman spectra of ZrO_2 (a), CeO_2 (b), $Ce_{0.8}Zr_{0.2}O_2$ (c), and $Ce_{0.2}Zr_{0.8}O_2$ (d). Samples c and d are obtained by milling an appropriate amount of CeO_2 and ZrO_2 for 9 h.

100–700 cm^{-1}, which probably belongs to a cubic, fluorite-structured phase. In the $Ce_{0.2}Zr_{0.8}O_2$ sample, the intensity of the 465 cm^{-1} band fades markedly and additional bands are observed at approximately 613, 316, 254, 142, and 117 cm^{-1}, as indicated in Fig. 5. The new spectral features are presumably due to a partial tetragonalization of the sample. It is known that Raman spectral features of tetragonal Ce–Zr–O samples are characterized by six bands in this region (29). The further three bands, located at 379, 191, and 179 cm^{-1}, indicate that a small amount of monoclinic ZrO_2 is still present. The low intensity and broadness of these peaks are probably caused by the small crystallites generated by mechanical milling. For very small crystallites (8–15 nm), the lack of long range order relaxes momentum conservation selection rules in the Raman scattering process, which results in a shift and broadness of the peaks (30). Unfortunately none of these data are known for Ce–Zr–O solid solution, which makes comparison impossible.

Morphological Features

The formation of solid solutions and morphological features were also studied by electron microscopy and EDX. The morphology of doped ceria powders was similar for the three samples. Figure 6 reports the SEM micrograph of $Ce_{0.8}Zr_{0.2}O_2$, which shows that the sample comprises an aggregation of packed particles only a few micrometers large. This is in agreement with previous observations of calcia- and magnesia-doped zirconia prepared by mechanical milling (19). Detailed HREM-EDX analysis was carried out to study the homogeneity of samples and the formation of true solid solutions. A typical electron micrograph obtained by HREM of mechanically alloyed Ce–Zr–O solid solution is shown in Figs. 7a and 7b. The sample comprises individual crystalline particles with sizes ranging from 4 to 15 nm. A considerable degree of lattice imperfection can be observed (see, for example, the arrows in Fig. 7b). The degree of imperfection can be explained by the mechanism responsible for material transfer during the milling process, which may include continuous bond rupture and formation, local temperature rises, microdeformation of the surface and hydrostatic stresses (31). EDX microanalysis performed on individual particles (probe size 5–8 nm) revealed in all cases the presence of a mixed oxide phase for Ce–Zr–O. Chemical composition within individual particles was kept constant as revealed by different sets of EDX profiles performed on individual grains. Homogeneity and composition from one grain to another was found to be within less than 10% deviation. A representative EDX profile corresponding to a single particle in the mechanically alloyed $Ce_{0.8}Zr_{0.2}O_2$ solid solution is shown in Fig. 8. No segregation of separate CeO_2 or ZrO_2 phases was observed in any case by EDX, which was consistent with selected-area diffraction experiments. However, a comparison with solid solutions prepared by conventional coprecipitation method did indicate a slightly lower degree of homogeneity, which can be partly eliminated by prolonging milling time. This lower homogeneity may be due to preferential enrichment of one of the two components in some areas of the material as a result of an incomplete reaction and/or the leaching

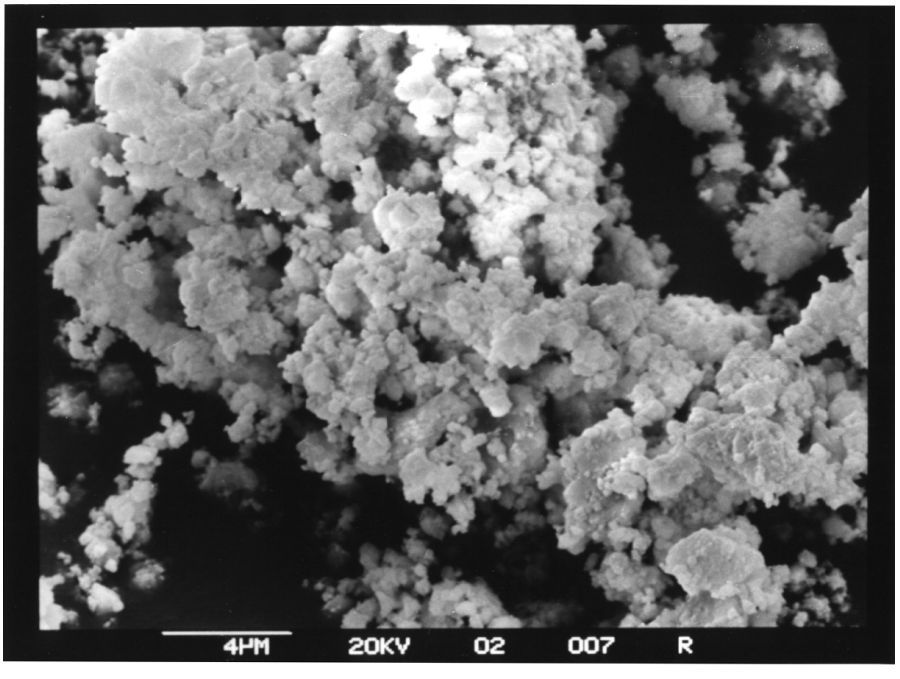

FIG. 6. SEM micrograph of $Ce_{0.8}Zr_{0.2}O_2$ obtained by MM.

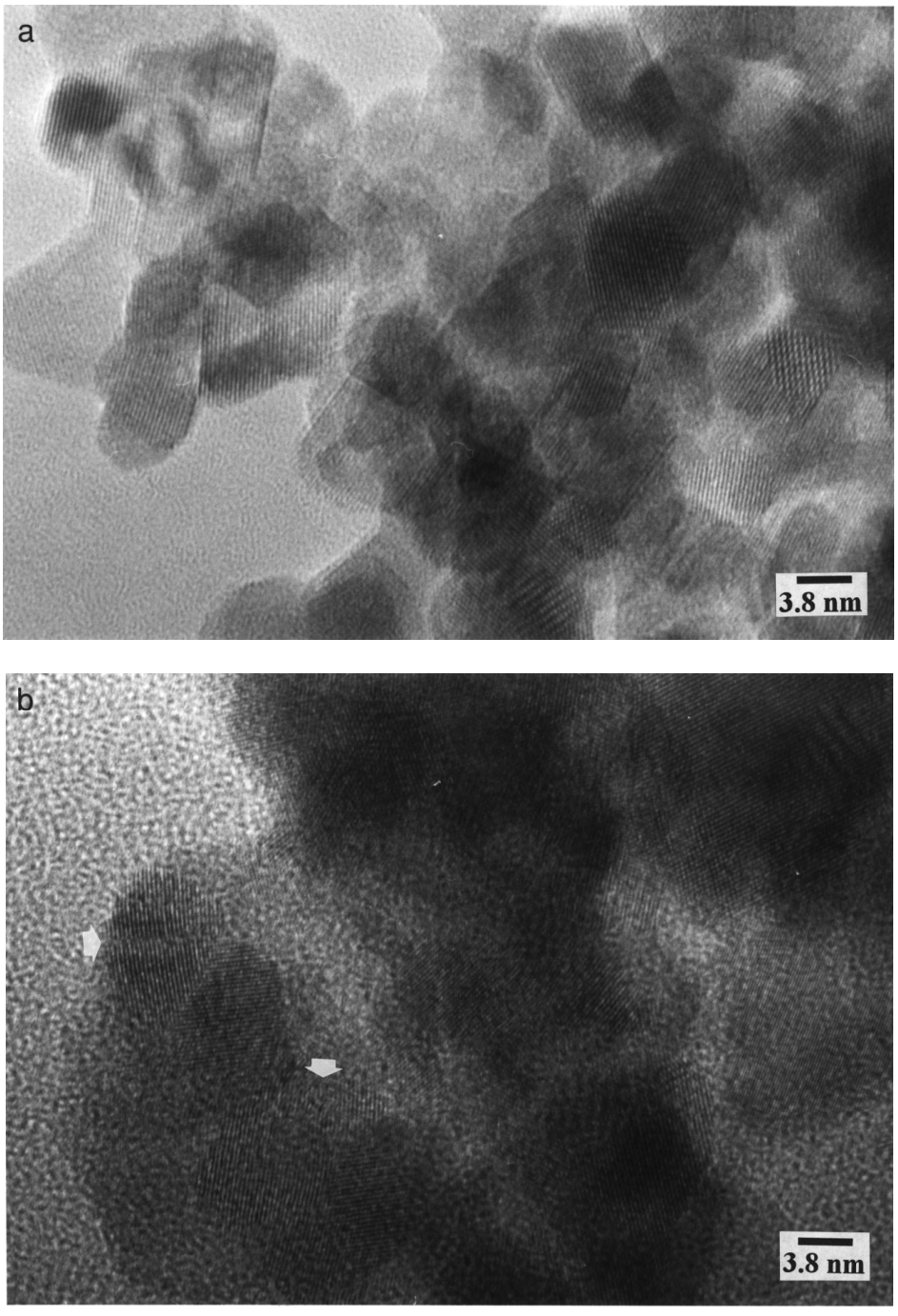

FIG. 7. Low magnification HRTEM image of $Ce_{0.8}Zr_{0.2}O_2$ solid solution obtained by mechanical milling for 9 h (a) showing lattice imperfection indicated by arrows (b).

of ZrO_2 from the apparatus (balls and vial). One of the major drawbacks of this methodology is the presence of impurities such as iron and tungsten from the milling media (17). To limit leaching, we used apparatus made from zirconia, which has two advantages over traditional metal devices. The loss of material from the balls is limited and in any case introduces not impurities as such but a modification in composition. Nevertheless, as can be verified by weight gain or loss after reaction, leaching from milling apparatus is limited to less than 1% (i.e., less than 10 mg for 1 g preparation).

Measurements of the Ce–Zr–O solid-solution lattice spacing were also performed on several crystallites representative of the $Ce_{0.8}Zr_{0.2}O_2$ sample (Fig. 9). This was

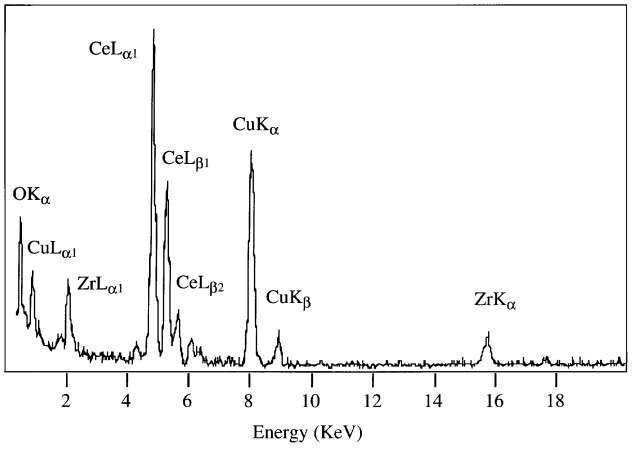

FIG. 8. Energy-dispersive X-ray profile corresponding to single particle of $Ce_{0.8}Zr_{0.2}O_2$ obtained by milling the reagents for 9 h. Copper signals are due to the grid used in the specimen preparation for electron microscopy.

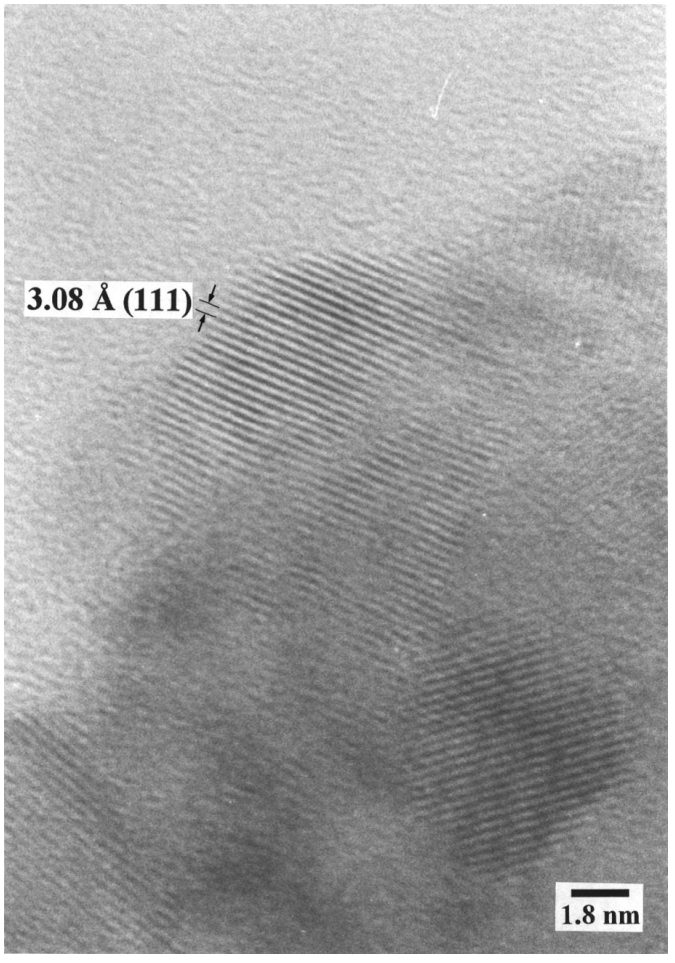

FIG. 9. High-magnification HRTEM image of $Ce_{0.8}Zr_{0.2}O_2$ particle showing {111} planes.

done by dividing the distance between the lateral faces of a given particle by the whole number of spacings as visualized by HREM. The average value for (111) lattice spacing was found to be 0.308 nm (corresponding to $a = 0.533$ nm). Taking into account that (111) lattice spacing for pure ceria is 0.312 nm ($a = 0.541$ nm), our estimate indicated a shrinking of the CeO_2 fluorite-type lattice when Zr^{4+} was introduced. This is consistent with XRD analysis, where a cubic lattice with $a = 0.5336(8)$ nm was found.

Hydrogen Uptake/Reduction Features

The introduction of ZrO_2 into the CeO_2 lattice has recently been reported to strongly affect the reduction features of ceria (3, 4). This occurs through structural modifications of the fluorite-type lattice of ceria as a consequence of the substitution of Ce^{4+} (ionic radius 0.97 Å) with Zr^{4+} (ionic radius 0.84 Å). The effect of this substitution is to decrease cell volume, lowering the activation energy for oxygen-ion diffusion within the lattice and consequently favoring reduction. The introduction of Zr also enhances the formation of structural defects which are expected to play an important role in determining reduction/oxidation behavior. We therefore analyzed the reduction features of mechanically alloyed Ce–Zr–O samples by studying their TPR profiles. The reduction profile of pure CeO_2 is characterized by two peaks (Fig. 10, curve a). There is one peak at temperature of ca. 800 K, which is strongly dependent

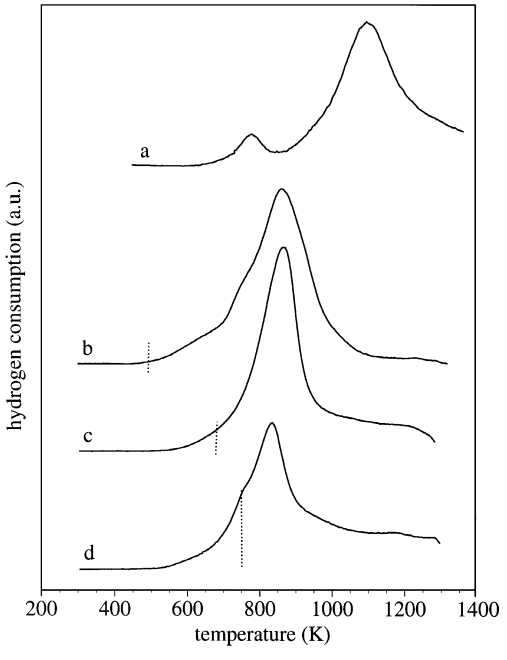

FIG. 10. TPR of CeO_2 (a), $Ce_{0.2}Zr_{0.8}O_2$ (b), $Ce_{0.5}Zr_{0.5}O_2$ (c), and $Ce_{0.8}Zr_{0.2}O_2$ (d). Samples b, c, and d are obtained by milling the appropriate amount of CeO_2 and ZrO_2 for 9 h. Dotted line indicates temperature at which hydrogen consumed equals that necessary for reduction of surface according to Ref. (35).

on surface area and which is generally attributed to the reduction of the uppermost layers of Ce^{4+} in CeO_2, and another peak at higher temperature originated by reduction of the material in the bulk (32). The overall degree of reduction is 48% at 1450 K, corresponding to the formation of CeO_x with $x = 1.76$. This was evaluated by integrating the TPR profile and by assuming that all adsorbed hydrogen contributes to ceria reduction. The TPR of mechanically alloyed ceria–zirconia samples shows completely different behavior (Figs. 10b–10d). The onset of H_2 consumption in solid solutions is observed at ca. 500 K, several degrees lower than in pure undoped CeO_2, and it is not severely influenced by cerium content. The appearance of this strong component of H_2 adsorption at lower temperatures can be related to several factors including a higher degree of surface Ce^{4+} reduction at lower temperatures and/or an increase of H_2 adsorption to produce hydride-like or bronze-like species in which hydrogen is inserted in the lattice (33, 34). High H_2 adsorption has recently been reported for Cu–Ce–O solid solutions in which stored hydrogen is then used to reduce cerium at lower temperatures (33). To estimate the amount of hydrogen required for reduction of surface Ce^{4+} in ceria–zirconia samples, we used the approach developed by Johnson and Mooi for pure CeO_2 (35). This method, which relies on the quantification of H_2 adsorbed by TPR, is not entirely beyond criticism as there is a possibility of other phenomena affecting overall H_2 consumption in high surface area samples (36). However the assumption that H_2 consumed in the first peak can be related to surface area has been successfully applied in some cases (37). It is evident that in our case the reduction of the first Ce^{4+} layer requires a negligible amount of hydrogen in comparison to H_2 adsorption responsible for the low-temperature TPR peak of ceria–zirconia. The temperature at which hydrogen consumption coincides with that required for reduction of all surface cerium is indicated in Fig. 10. Clearly no separation between surface and bulk reduction can be made. We therefore attributed increased H_2 adsorption mainly to reduction of Ce^{4+} on both surface and bulk as a result of an increase in the oxygen diffusion rate, although we cannot exclude that some adsorbed hydrogen could be stored first and only desorbed or consumed for reduction subsequently. The lower oxygen mobility in the bulk and the low surface area could account for the absence of low temperature features in pure CeO_2. The degree of reduction of Ce^{4+} at 1450 K, as estimated by integration, ranges from 66% in $Ce_{0.8}Zr_{0.2}O_2$ to 89% in $Ce_{0.2}Zr_{0.8}O_2$ and it is better detailed in Table 1.

The formation of solid solution in the mill is very well highlighted by monitoring the H_2 consumption in the TPR of a mixture of 50 mol% of CeO_2 and 50 mol% of ZrO_2 subjected to different milling times. This is reported in Fig. 11 for samples milled from 0 to 8 h. The simple mixture of CeO_2 and ZrO_2 shows a TPR profile which is similar to that of pure ceria, since ZrO_2 does not show any H_2 uptake in this region. As the milling time increases there is a lowering of the intensity of this peak simultaneously with the enhancement of the low-temperature peak. This causes strong promotion of hydrogen uptake in milled samples particularly in the 800–1100 K region, where the effect of milling is evident (see Fig. 12). The reason for this enhancement is the gradual introduction of Zr into CeO_2 lattice, with a concurrent reduction of particle size down to a few nanometers, a process which is complete in about 9 h, as is demonstrated by X-ray analysis.

TABLE 1

Surface Area and Reduction Features of Ce–Zr–O Prepared by MM

Sample	Surface area,[a] m^2/g	H_2 consumed, $\mu mol/g$[b]	x in CeO_x–ZrO_2[c]	y in $CeZrO_y$[d]
CeO_2	5–18	1336(93)	1.76	1.76
$Ce_{0.8}Zr_{0.2}O_2$[e]	27–33	1626(114)	1.67	1.736
$Ce_{0.5}Zr_{0.5}O_2$[e]	16–20	1388(97)	1.59	1.795
$Ce_{0.2}Zr_{0.8}O_2$[e]	9–13	669(47)	1.555	1.911
$Ce_{0.65}Zr_{0.35}O_2$[e]	14–18	—	—	—
$Ce_{0.9}Zr_{0.1}O_2$[e]	20–25	—	—	—
ZrO_2	27	—	—	—

[a] The samples are made in 1–2 g batches. These data specify the range of surface areas obtained within several repeated preparations. In the case of CeO_2 the different areas correspond to different lot numbers.

[b] The H_2 uptake was calculated by integration of the TPR profile; the error is reported in parentheses.

[c] Extent of reduction of CeO_2 in Ce–Zr–O solid solutions.

[d] Overall reduction in Ce–Zr–O solid solutions.

[e] Milling time, 9 h.

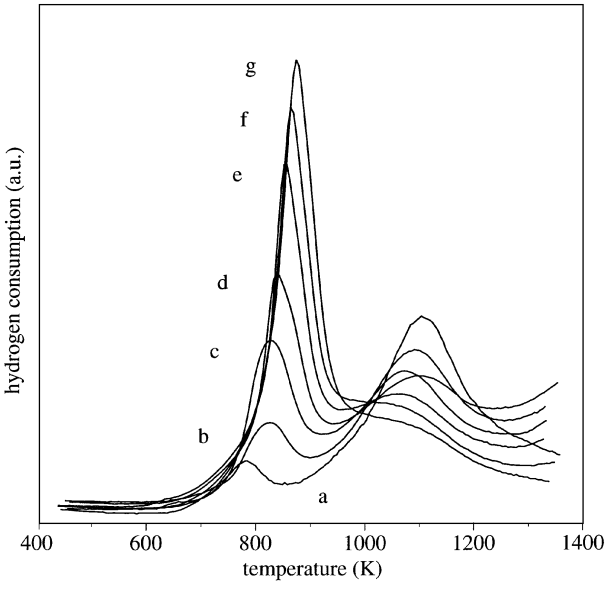

FIG. 11. TPR of mixture of 50% mol CeO_2 and 50% mol ZrO_2 milled for 0 (a), 0.5 (b), 1 (c), 2 (d), 3 (e), 5 (f), and 9 h (g).

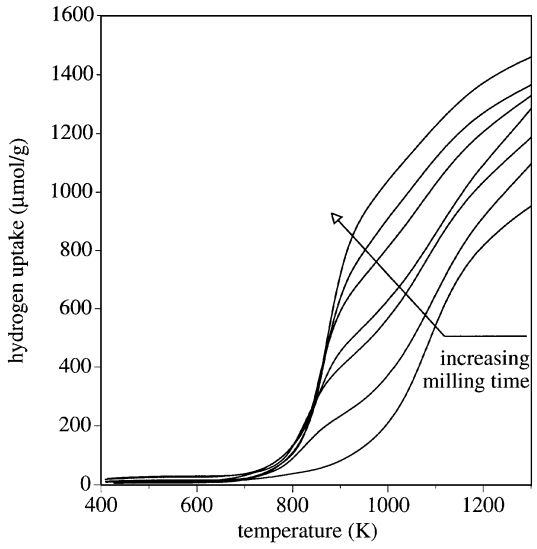

FIG. 12. Hydrogen consumption calculated from TPR of mixture of 50% mol CeO_2 and 50% mol ZrO_2 milled for 0, 0.5, 1, 2, 3, 5, and 9 h.

In order to understand how milling (and not the chemical nature) of the material could modify the redox behavior we carried out a TPR analysis on a sample of CeO_2 and $Ce_{0.5}Zr_{0.5}O_2$ prepared by conventional coprecipitation and then subjected to ball milling for 9 h. The results are reported in Fig. 13. The reduction features of CeO_2 and of $Ce_{0.5}Zr_{0.5}O_2$ are not strongly modified; an increase of the low-temperature feature is observed on CeO_2 (attributable to an increase of surface area induced by milling, 6 vs 28 m^2/g), while only a small shift of the maximum of the reduction peak is observed over $Ce_{0.5}Zr_{0.5}O_2$. This indicates that the structural defects created by milling do not strongly modify the redox behavior of Ce–Zr–O solid solutions. It is likely that under the conditions (especially high temperature) typical of a TPR analysis, defects created by milling rearranges to more stable, defect-free structures. Therefore, it is mainly the chemical/structural nature of the compounds, more than the presence of defects induced by milling which determines the redox properties of the material, at least for this range of temperatures.

Another interesting feature of CeO_2–ZrO_2 solid solutions is their unusual redox behavior after high-temperature redox cycling (10, 12), that is the reduction of Ce^{4+} in solid solution is not affected (12) or even promoted (10) if samples are thermally treated at high temperatures. This feature was tested also in our samples prepared by mechanical milling. Figure 14 shows the repeated TPR cycles of a mixture of 50% CeO_2–50% ZrO_2 after 0.5, 2, 4, and 9 h of milling. In this case the samples have been subjected to the following procedure: (i) milling for the time indicated, (ii) first TPR from 300 to 1450 K, (iii) oxidation at 773 K under air, and (iv) second TPR. As can be seen the first treatment under TPR conditions does not influence the hydrogen uptake at low temperature, although the surface areas are strongly influenced by the thermal treatment (they drop to less than 2 m^2/g for all samples). This is in contrast to what happens with pure ceria, in which thermal treatments strongly affect redox behavior and repeated TPR cycles dramatically reduce hydrogen adsorption at lower temperature (10, 12). In this case almost the opposite behavior is observed, the residual high-temperature feature of the CeO_2–ZrO_2 mixture milled for 9 h disappeared after the first thermal cycle. This can be explained by a slight rearrangement of atoms from their original position driven

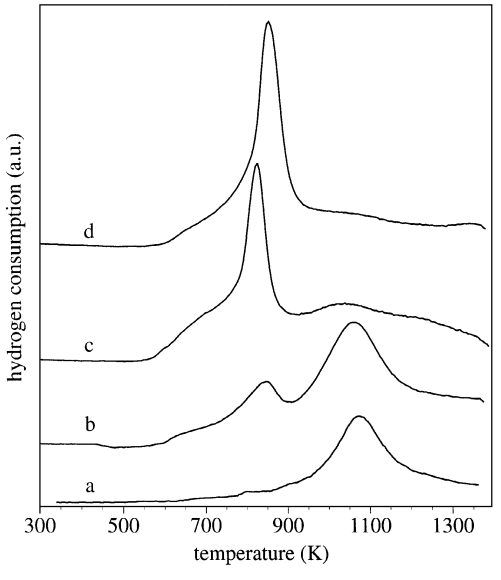

FIG. 13. Effect of milling on the TPR of ceria and ceria–zirconia prepared by conventional route. (a) TPR of CeO_2 (Aldrich, 6 m^2/g), (b) TPR of sample a after milling for 9 h; (c) TPR of $Ce_{0.5}Zr_{0.5}O_2$ prepared by coprecipitation (68 m^2/g); (d) TPR of sample c milled for 9 h.

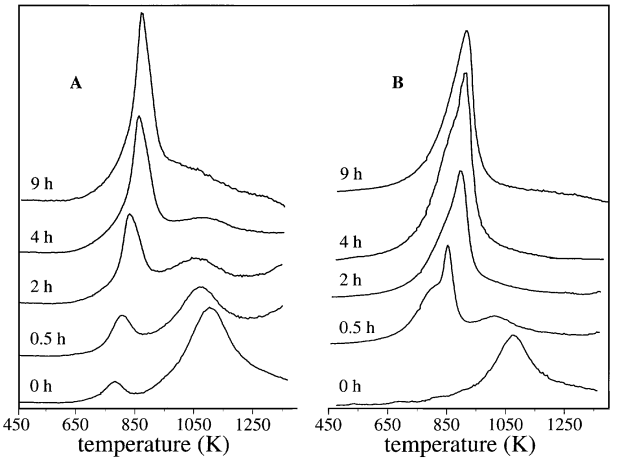

FIG. 14. TPR of mixture of 50% mol CeO_2 and 50% mol ZrO_2 milled for 0, 0.5, 2, 4, and 9 h. Fresh samples (A) and recycled samples (B).

by temperature (10) or by a more complete degree of formation of solid solution induced by treating at 1450 K. As a matter of fact, samples milled for 0.5 and 2 h, under conditions where solid solution cannot be completely formed, strongly increase their reduction features at low temperature after the first TPR. Overall this remarkable redox behavior, which is unaffected by textural properties, and thus not dependent on surface area, can be explained by the increase of bulk anion mobility into a modified ceria.

Oxygen Storage/Release Properties

One of the main roles of ceria in auto-exhaust catalysts is that of rapidly switching between CeO_2 and CeO_{2-x} under lean and rich conditions, respectively (2). In pure ceria, this process is strongly dependent on surface redox phenomena (38). A reduction of surface area therefore has a negative impact on the capacity to rapidly store and release oxygen. With the introduction of dopants into the CeO_2 lattice there are at least two beneficial effects: (i) an increase in thermal stability which reduces surface-area loss upon aging; and (ii) an increased diffusion rate of oxygen which positively influences the rapid exchange of oxygen, not only on the surface but throughout (3, 5, 39). High oxygen storage capacity should enlarge the operating A/F window without negatively affecting TWC performances. We therefore studied the oxygen storage/release behavior of CeO_2–ZrO_2 mixed oxides prepared by mechanical milling under conditions in which OSC is either limited by thermodynamic factors (i.e., number of oxygen vacancies) or is kinetically controlled. The former gives an estimate of the total O_2 that can be exchanged following reduction and depends on the total number of reduced accessible sites present on the catalyst (for example oxygen vacancies or Ce^{3+} in CeO_2), while the latter involves measuring oxygen that is kinetically accessible under conditions which are typical of auto-exhaust catalysts, i.e., rapid oscillations of the gas mixture from a reducing to an oxidizing environment.

Total OSC for $Ce_xZr_{1-x}O_2$ is reported in Fig. 15. As indicated under Experimental, between reduction and oxidation the sample was treated under inert flow at temperatures varying from 650 to 873 K. This was done in order to ascertain whether H_2 adsorption/desorption could affect OSC measurements. The oxygen uptake values were unaffected by thermal treatments, indicating that reaction of adsorbed H_2 with O_2 is unlikely under these conditions. This is also consistent with the relatively low surface area of our samples and with the observation that H_2 adsorption on CeO_2 is strongly dependent on textural properties (40). Two sets of data are represented in Fig. 15 to show the oxygen adsorbed per gram of catalyst and per cerium atom. Oxygen adsorption is at a minimum with pure CeO_2 (ZrO_2 does not show any adsorption) and it gradually increases with the introduction of ZrO_2. Oxygen consumption, either calculated on a per gram or on a per mole of Ce basis, is influenced by

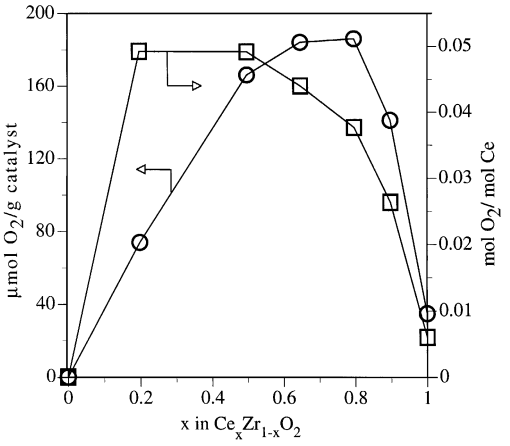

FIG. 15. Total oxygen storage capacity of $Ce_xZr_{1-x}O_2$ calculated on per gram basis (○), and on per cerium atom basis (□). Samples obtained after 9 h of milling.

the formation of solid solutions. Whereas in the first case a maximum is observed for $Ce_xZr_{1-x}O_2$ with $0.6 \leq x \leq 0.8$, the composition giving the largest adsorption per mole of Ce is in the range $x = 0.2$–0.5. These results are in agreement with the data obtained by TPR analysis. The lower the cerium content, the higher the degree of reduction of Ce^{4+} in solid solution. The total oxygen consumption needed for reoxidation calculated per cerium atom is therefore expected to increase at low Ce concentrations. Conversely, the oxygen consumed per gram of catalyst increases as the concentration of redox sites on the samples rises, although the degree of reduction of Ce^{4+} is lower.

A rather different picture is observed if only the kinetically accessible OSC is measured (Fig. 16). In this case, regardless of the set of data considered, a maximum of O_2 adsorption is observed at higher Ce content, with a

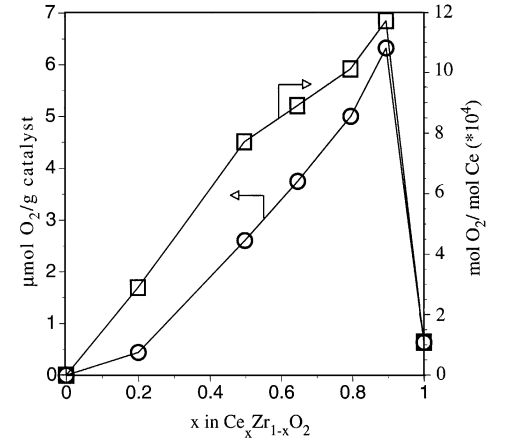

FIG. 16. Dynamic oxygen storage capacity of $Ce_xZr_{1-x}O_2$ calculated on per gram basis (○) and on per cerium atom basis (□). Samples obtained after 9 h of milling.

composition $Ce_{0.9}Zr_{0.1}O_2$, even though there is no substantial difference in samples with $x = 0.5$–0.9. This means that in CeO_2-rich ceria–zirconia solid solutions, oxygen is much more readily and rapidly available than in samples where ZrO_2 content exceeds 50%. These data are in qualitative agreement with those recently reported by Cuif *et al.* (14) where OSC was found to have a maximum at the composition $Ce_{0.6}Zr_{0.4}O_2$. In the above case, however, the amount of adsorbed oxygen differs considerably from our findings, a result which may be attributed to different experimental conditions (temperature and reductant/oxidant concentration) and the different methods employed for catalyst preparation. Similar systems have been recently analyzed also by Tanaka *et al.* (41). They found that fresh, Pt-loaded $Ce_{0.8}Zr_{0.15}Y_{0.05}$ has the best OSC behavior compared to catalysts having lower cerium content. The effect of thermal treatment in this case is to reduce oxygen adsorption capacity, especially, of samples having high cerium loading. An enhancement of the H_2 uptake and a beneficial effect of CeO_2–ZrO_2 solid solution on the performances of Pt,Rh TWC catalysts has been also recently reported by Nunan *et al.* (13) which found that on aged catalysts, the introduction of more than 18% of ZrO_2 into CeO_2 lattice produces important advantages on the chemical promotional effect of CeO_2, particularly with CO/NO mixtures. Likewise, Ranga Rao *et al.* (15) found a strong enhancement of NO decomposition rate over $Rh/Ce_{0.6}Zr_{0.4}O_2$ reduced at 673 K, compared to Rh/CeO_2; the driving force for this enhancement was attributed to the formation of oxygen vacancies and to their participation in the catalytic cycle. The choice of this composition was done on the basis of the observed redox behavior, which showed a maximum over cubic $Ce_xZr_{1-x}O_2$ with $x = 0.4$–0.5 (3). Moreover, previous results (12) indicated that the introduction of 20 mol% ZrO_2 into CeO_2 strongly affects the kinetic of oxygen adsorption by lowering the activation energy for O_2 uptake.

Overall previous results seem to indicate that there is a broad range of composition where the oxygen adsorption and catalytic features are influenced by formation of solid solution. These compositions are dependent on several parameters such as the preparation method, which should allow formation of a mixed oxide phase, the aging temperature, which affect textural and morphological features, and/or the presence of noble metals, which enhances oxygen adsorption by cooperating synergetically with the support. In the present case, where thermal treatments are not employed and in the absence of noble metals, the number of variables reduces and the structural factors should play the most important role.

To explain the different results obtained under dynamic conditions, we need answer to the following questions: (i) why does $Ce_{0.2}Zr_{0.8}O_2$ show extremely poor O_2 adsorption under a kinetically controlled regime even when calculated on a Ce basis? (ii) why are the best performances obtained with Ce-rich samples? To answer these questions fully, we need to consider several important aspects in the development of these materials, especially the structural features and the role of the various components in the mixed oxide.

The reoxidation of Ce in Ce–Zr–O mixed oxides depends on a number of factors including the participation at various stages of the surface and the bulk of the oxide. The first step is the surface activation of oxygen which may occur through several intermediates depending on the electron donor ability of the ceria surface and gives as a final species a double charged oxygen anion (2):

$$O_{2ads} \cdots \overset{+4e^-}{\rightleftharpoons} \cdots 2O^{2-}$$

This process is followed by the migration of oxygen ions into the bulk which, for a defective fluorite-structured solid solution, can be described by a vacancy mechanism. It is therefore expected that the smaller the cell volume, the lower the energy required to hop oxygen through the lattice. This would imply that an increase in ZrO_2 content will always produce an observable increase in dynamic OSC, which is in contradiction with experimental results. Consequently, additional factors must be considered to explain this behavior. Structural analysis has shown that for low CeO_2 content, it is likely that under milling conditions the formation of tetragonal solid solution takes place. Oxygen diffusion in a tetragonal structure should be hindered for two reasons. The first is the anisotropy of diffusion, which will limit the overall diffusion rate in a polycrystalline material because of the different orientation of the grain boundaries (3). The second reason is the effective dimension of the channel radius through which oxygen migrates, which is favored for a cubic structure. This could explain the poor OSC behavior observed in $Ce_{0.2}Zr_{0.8}O_2$ but not the excellent oxygen adsorption of cubic, CeO_2-rich, samples. A possible explanation for this behavior may lie in the consideration that the transfer of oxygen anions into the bulk must be accompanied by a counterflow of electrons towards the surface (42). This requires the presence of chains of ions with redox properties. In the present case, only Ce can help charge transfer by electron exchange in accordance with the following equations, which are similar to those described by Sinev *et al.* for Pr-based oxides (42):

$$Ce_a^{4+} + Ce_b^{3+} \rightleftharpoons Ce_a^{3+} + Ce_b^{4+}$$

$$Ce^{4+} + O^{2-} \rightleftharpoons Ce^{3+} + O^-$$

It is therefore expected that the presence of chains of neighboring Ce atoms will accelerate the process. On decreasing Ce content, a decrease in the average distance between cerium atoms should hinder electron transfer in the lattice with a negative effect on oxygen adsorption capabilities and so explain the increase in OSC that accompanies

an increase in cerium content. Another contribution to electronic conductivity may come from the dimensions of the crystallites prepared by mechanical milling. It has recently been reported that the transport properties of nanocrystalline CeO_{2-x} are greatly enhanced by reduced resistance in grain boundaries and higher electronic conductivity (43). These properties, which are attributed to the formation of interfacial defects, are also expected to play an important role here, where materials with a high number of defects are generated. The presence of defects and lattice mismatch in the development of materials with a high oxygen storage/release capacity has also been recognized by Egami *et al.* (44), who found that the presence of nanoscale segregated CeO_2 phase in close contact with ZrO_2 and/or CeO_2–ZrO_2 enhances the OSC of ceria–zirconia mixtures. The authors attributed the redox behavior of a nonhomogeneous Ce–Zr–O solid solution to an unusual nanoscale phase segregation of CeO_2 with exposure of high-energy surfaces, where O_2 removal is favored, therefore minimizing the importance of having an homogeneous single phase.

Mechanics of the Milling Process

Although the main purpose of this paper was to present a novel method for preparing ceria–zirconia mixed-oxide catalysts with a high oxygen storage capacity and enhanced redox features, we would like to focus here on the mechanisms that may be considered to explain the process.

In the mill the central event which determines microscopic deformation, with continuous bond rupture and formation, is the ball-powder-ball collision. These collisions are, in turn, influenced by several macroscopic parameters such as oscillation frequency, milling media, charge ratio (total ball mass/powder mass) and time. Under our experimental conditions the number of ball-to-ball impacts may be estimated at around 800/sec (31). Therefore, in a 9-h experiment, approximately 25 million collisions will take place. If we assume that every collision is effective in inducing breaking and welding of particles, this number is not high enough to explain an homogeneous formation of a mixed-oxide phase. Other factors must also be considered. Since melting, mixing, and solidification is the most important sequence that leads to the formation of solid solution, one possible mechanism is the local surface melting that occurs during impaction of the powder. Although this assumption is reasonable, it must be excluded because of the high temperatures that would be required for the process and which are well above those estimated for a mill. Local powder temperature rises during impact resulting from the kinetic energy of the milling balls cannot be higher than 200–300 K and are not therefore sufficient to induce oxide surface melting. However, this local temperature rise can induce an enhancement of microdiffusion and plastic deformation even in brittle materials (31) which can contribute to the formation of a mixed-oxide phase. Thus even if not all the collisions contribute to the formation of solid solutions, it will be necessary for a few to possess sufficient kinetic energy to produce the temperature rises necessary for mechanical alloying to take place.

CONCLUSIONS

Summarizing, mechanical milling is an appropriate new tool for preparing mixed-oxide catalysts with redox behavior similar to that observed over solid solutions prepared by conventional methods. The following factors need to be highlighted:

- Dissolution of ZrO_2 into CeO_2 lattice was observed in all the composition range with formation of a fluorite-structured, cubic solid solution for ZrO_2 content not exceeding 50 mol% and with a partial tetragonalization for higher zirconium loading.
- The formation of solid solution was followed by X-ray diffraction and temperature-programmed reduction. A strong enhancement of the redox properties of CeO_2 was observed by introduction of ZrO_2.
- The capacity of reversibly adsorbing oxygen was also measured. Under dynamic conditions CeO_2-rich solid solutions showed the best behavior, which can be correlated to a high oxygen mobility and to the presence of a large number of atoms with redox character.

Finally, the possibility of modifying lattice oxygen mobility and the kinetic of Ce(IV) reduction by introduction of small quantities of dopants is a powerful additional tool in the design of innovative catalytic materials with elevated oxygen storage/transport capacity.

ACKNOWLEDGMENTS

The authors thank MURST and CNR for financial support. MEL chemicals (UK) is also acknowledged for providing samples of zirconia. The FT-Raman spectrometers were purchased with the help of the PHARE-ACCORD Program H-9112-0152.

REFERENCES

1. Taylor, K. C., "Catalysis, Science and Technology" (J. R. Anderson and M. Boudart, Eds.), p. 119. Springer Verlag, Berlin, 1984.
2. Trovarelli, A., *Catal. Rev.-Sci. Eng.* **38**, 439 (1996).
3. Fornasiero, P., Di Monte, R., Ranga Rao, G., Kaspar, J., Meriani, S., Trovarelli, A., and Graziani, M., *J. Catal.* **151**, 168 (1995).
4. Murota, T., Hasegawa, T., Aozasa, S., Matsui, H., and Motoyama, M., *J. Alloys Comp.* **193**, 298 (1993).
5. Cho, B. K., *J. Catal.* **131**, 74 (1991).
6. Logan, A. D., and Shelef, M., *J. Mater. Res.* **9**, 468 (1994).
7. Zamar, F., Trovarelli, A., de Leitenburg, C., and Dolcetti, G., *Stud. Surf. Sci. Catal.* **101**, 1283 (1996).
8. Zhang, Y., Andersson, A., and Muhammed, M., *Appl. Catal. B: Environ.* **6**, 325 (1995).
9. Pijolat, M., Prin, M., Soustelle, M., Touret, O., and Nortier, P., *J. Chem. Soc. Faraday Trans.* **91**, 3941 (1995).

10. Fornasiero, P., Balducci, G., Di Monte, R., Kaspar, J., Sergo, V., Gubitosa, G., Ferrero, A., and Graziani, M., *J. Catal.* **164**, 173 (1996).
11. Zamar, F., Trovarelli, A., de Leitenburg, C., and Dolcetti, G., *J. Chem. Soc. Chem. Commun.* 965 (1995).
12. de Leitenburg, C., Trovarelli, A., Llorca, J., Bini, G., and Cavani, F., *Appl. Catal. A: Gen.* **139**, 161 (1996).
13. Nunan, J. G., Williamson, W. B., and Robota, H. J., SAE Paper 960798, 1 (1996).
14. Cuif, J., Blanchard, G., Touret, O., Marczi, M., and Quéméré, E., SAE Paper 961906, 73 (1996).
15. Ranga Rao, G., Fornasiero, P., Di Monte, R., Kaspar, J., Vlaic, G., Balducci, G., Meriani, S., Gubitosa, G., Cremona, A., and Graziani, M., *J. Catal.* **162**, 1 (1996).
16. Sun, Y., and Sermon, P. A., *J. Mater. Chem.* **6**, 1025 (1996).
17. Koch, C. C., and Whittenberger, J. D., *Intermetallics* **4**, 339 (1996).
18. Benjamin, J. S., *Metall. Trans.* **1**, 2943 (1970).
19. Zazhigalov, V. A., Haber, J., Stoch, J., Bogutskaya, L. V., and Bacherikova, I. V., *Appl. Catal. A: Gen.* **135**, 155 (1996).
20. Mori, S., Xu, W.-C., Ishidzuki, T., Ogasawara, N., Imai, J., and Kobayashi, K., *Appl. Catal. A: Gen.* **137**, 255 (1996).
21. Trovarelli, A., Matteazzi, P., Dolcetti, G., Lutman, A., and Miani, F., *Appl. Catal. A: Gen.* **95**, L9 (1993).
22. Michel, D., Faudot, F., Gaffet, E., and Mazerolles, L., *J. Am. Ceram. Soc.* **76**, 2884 (1993).
23. Chen, Y. L., Qi, M., and Yang, D. Z., and Wu, K. H., *Mater. Sci. Eng. A* **183**, L9 (1994).
24. de Leitenburg, C., Trovarelli, A., Zamar, F., Maschio, S., Dolcetti, G., and Llorca, J., *J. Chem. Soc. Chem. Commun.* 2181 (1995).
25. Trovarelli, A., de Leitenburg, C., Dolcetti, G., and Llorca, J., *J. Catal.* **151**, 111 (1995)
26. Kim, D.-J., *J. Am. Ceram. Soc.* **72**, 1415 (1989).
27. Yashima, M., Arashi, H., Kakihana, M., and Yoshimura, M., *J. Am. Ceram. Soc.* **77**, 1067 (1994).
28. Keramidas, V. G., and White, W. B., *J. Am. Ceram. Soc.* **57**, 22 (1974).
29. Kim, D.-J., Jung, H.-J., and Yang, I.-N., *J. Am. Ceram. Soc.* **76**, 2106 (1993); Hirata, T., Asari, E., and Kitajima, M., *J. Solid State Chem.* **110**, 201 (1994).
30. Richter, H., Wang, Z. P., and Levy, L., *Solid State Commun.* **39**, 625 (1981).
31. Davis, R. M., McDermott, B., and Koch, C. C., *Metall. Trans. A* **19A**, 2867 (1988).
32. Yao, H. C., and Yao, Y. F. Y., *J. Catal.* **86**, 254 (1984).
33. Wrobel, G., Lamonier, C., Bennani, A., D'Huysser, A., and Aboukaïs, A., *J. Chem. Soc. Faraday Trans.* **92**, 2001 (1996).
34. Cunningham, J., O'Brien, S., Sanz, J., Rojo, J. M., Soria, J. A., and Fierro, J. L. G., *J. Mol. Catal.* **57**, 379 (1990).
35. Johnson, M. F. L., and Mooi, J., *J. Catal.* **103**, 502 (1987); Johnson, M. F. L., and Mooi, J., *J. Catal.* **140**, 612 (1993).
36. Zotin, F. M. Z., Tournayan, L., Varloud, J., Perrichon, V., and Frety, R., *Appl. Catal. A: Gen.* **98**, 99 (1993).
37. Perrichon, V., Laachir, A., Bergeret, G., Fréty, R., Tournayan, L., and Touret, O., *J. Chem. Soc. Faraday Trans.* **90**, 773 (1994).
38. Schmieg, S. J., and Belton, D. N., *Appl. Catal. B: Environ.* **6**, 127 (1995).
39. Miki, T., Ogawa, T., Haneda, M., Kakuta, N., Ueno, A., Tateishi, S., Matsura, S., and Sato, M., *J. Phys. Chem.* **94**, 6464 (1990).
40. Bernal, S., Calvino, J. J., Cifredo, G. A., Gatica, J. M., Perez Omil, J. A., and Pintado, J. M., *J. Chem. Soc. Faraday Trans.* **89**, 3499 (1993).
41. Tanaka, H., and Yamamoto, M., SAE Paper 960794, 231 (1996).
42. Sinev, M. Yu., Graham, G. W., Haach, L. P., and Shelef, M., *J. Mater. Res.* **11**, 1960 (1996).
43. Chiang, Y.-M., Lavik, E. B., Kosacki, I., Tuller, H. L., and Ying, J. Y., *Appl. Phys. Lett.* **69**, 185 (1996).
44. Egami, T., Dmowski, W., and Brezny, R., SAE Paper 970461, 000 (1997).